Surface & Coatings Technology 257 (2014) 3–14

Contents lists available at ScienceDirect

Surface & Coatings Technology

journal homepage: www.elsevier.com/locate/surfcoat

Crossover of texture and morphology in $(Ti_{1-x}Al_x)_{1-y}Y_yN$ alloy films and the pathway of structure evolution

L. Székely [a], G. Sáfrán [a], V. Kis [a], Z.E. Horváth [a], P.H. Mayrhofer [b], M. Moser [c], G. Radnóczi [a], F. Misják [a], P.B. Barna [a,*]

[a] Research Centre for Natural Sciences, Institute for Technical Physics and Materials Science, Konkoly-Thege M.u. 29-33, H-1121 Budapest, Hungary
[b] Institute of Materials Science and Technology, Vienna University of Technology, 1040 Vienna, Austria
[c] Department of Physical Metallurgy and Materials Testing, Montanuniversität Leoben, Franz-Josef-Str. 18, A-8700 Leoben, Austria

ARTICLE INFO

Available online 6 September 2014

Keywords:
TiAlN
Texture crossover
Phase separation
Spinodal decomposition
Structure evolution
Competitive growth

ABSTRACT

In our earlier published work, we have shown that there is a composition range of the $(Ti_{1-x}Al_x)_{1-y}Y_yN$ alloy films ($0.72 < Ti/Al < 0.88$) deposited at oblique vapour beam incidence and 500 °C (corresponding to zone T) in which mixed cubic TiN (c-TiN) and wurtzite AlN (w-AlN) structures were formed together with an unusual complex texture. The texture of c-TiN phase changed from ⟨001⟩ to <111> at a certain thickness forming a definite crossover. Moreover the c-TiN<111> and the w-AlN⟨0001⟩ crystals were epitaxially related with axes tilted to the direction of the vapour beam.

Based on a comprehensive transmission electron microscopy (TEM) and diffraction (XRD and selected area electron diffraction (SAED)) structure and morphology analysis, we discovered the details of this exotic structure making it possible to construct the complex pathway of structure evolution including the formation of the w-AlN phase and the change of the dominating texture of c-TiN phase with thickness in dependence of the Ti/Al ratio and the deposition parameters. This pathway could be deduced from the fundamental phenomena of structure formation and may be generalised for multi-component thin film systems. A composition structure zone model has been also proposed for the $(Ti_{1-x}Al_x)_{1-y}Y_yN$ thin film system in the $0 < x < 1$ composition range.

1. Introduction

Understanding the variation of the texture with film thickness (manifested in an *orientation crossover*) identified at first in TiN films [1,2] without changing the parameters during film deposition raised a high interest and initiated a broad discussion in the last decades. The first idea proposed to interpret the formation of this specific structure was a possible restructuring as a result of the minimization of the overall energy of the film which is increasing with film thickness [1]. A detailed analysis of the proposed ideas on the possible mechanisms developing this kind of crossover is given in [3]. The main problem of these ideas was, however, that they were not based on detailed structure analysis of the films which could confirm their validity.

Orientation crossover has been indicated in TiAlN films by in situ synchrotron experiments also in the composition range where a two-phase (cubic, c-TiN and wurtzite, w-AlN) structure developed [4]. These authors investigated, however, only the first stages of film formation (up to 0.2 μm), therefore they could detect only that the first developing ⟨001⟩ texture started to change to the ⟨111⟩. Shetty and Karimi [5] illustrated the crossover between the first developed c-TiN⟨001⟩ and the next c-TiN⟨111⟩ textures in thick (4.5 μm) single phase TiAlN film, deposited at high (possibly 650 °C) substrate temperature. A crossover-like change in the orientation of c-TiN phase has been demonstrated in the 1.5–2 μm thick $(Ti_{1-x}Al_x)_{1-y}Y_yN$ films prepared at 500 °C substrate temperature at oblique vapour beam incidence in the composition range in which the two-phase structure (cubic-TiN and wurtzite-AlN) developed and has been published in our earlier papers [6,7]. In these experiments a single phase c-TiAlN structure with V-shaped columnar morphology and ⟨001⟩ texture has been found at $Ti/Al \geq 0.88$. However, in the $0.72 < Ti/Al < 0.88$ composition range, beside the c-TiN the w-AlN phase with tilted ⟨0001⟩ texture could be also detected in increasing fraction by selected area electron diffraction (SAED) analysis of cross sectional specimens when the Al concentration increased. The peculiarity of this structure was that this w-AlN texture was connected in each case to a c-TiN texture with $\{111\}_{TiN}//\{0001\}_{AlN}$ and $\langle 110\rangle_{TiN}//\langle 11\text{-}20\rangle_{AlN}$ epitaxial relation resulting in a <111>c-TiN//⟨0001⟩w-AlN fibre texture. According to the preliminary SAED investigations the <111>c-TiN//⟨0001⟩w-AlN was the only texture in the upper thickness range of the film, while in the lower thickness range the ⟨001⟩c-TiN and the <111>c-TiN//⟨0001⟩ w-AlN textures coexisted. The dominance of the ⟨001⟩c-TiN texture decreased with increasing Al concentration. Moreover, the axis of the <111>c-TiN//⟨0001⟩w-AlN texture was tilted to the direction of the incident vapour beam. These

* Corresponding author.
E-mail address: barna.peter@ttk.mta.hu (P.B. Barna).

http://dx.doi.org/10.1016/j.surfcoat.2014.08.071
0257-8972/

peculiarities suggested also the existence of a "crossover" from ⟨001⟩ to <111>c-TiN textures. It was intriguing that with increasing Al concentration the "crossover thickness" (the thickness at which the "crossover" appeared) decreased. Because the crossover in the c-TiN texture showed up simultaneously with the w-AlN, this phenomenon has been attributed to the formation of the wurtzite phase together with the oblique deposition. However, in lack of the necessary structure information, the real mechanisms controlling the development of this complex structure and texture could not be given in Ref. [7]. An additional more complex and detailed structure analysis of the two-phase $(Ti_{1-x}Al_x)_{1-y}Y_yN$ films was strongly stimulated also by the hope that the description and understanding of the evolution of this complex structure could discover some new mechanisms and pathways of structure evolution which might have a general force in controlling the structure evolution of multi-component films.

The phase composition of the polycrystalline $(Ti_{1-x}Al_x)_{1-y}Y_yN$ films in dependence of the Ti/Al ratio has been investigated both in as-deposited and heat treated films. The early work of Wahlström et al. [8] discovered the phase composition and texture relations in the $0 \le x \le 1$ composition range in the as deposited films. They have found three distinct composition ranges: c-TiAlN single phase, c-TiAlN + w-AlTiN two-phase and w-AlTiN single phase structures, respectively. In the first range the cubic ⟨001⟩, in the third the wurtzite ⟨0001⟩ textures dominated. A drastic reduction of the grain size and that of the intensity of XRD pattern have been found in the two-phase range. The formation of the w-AlN phase in the two-phase composition range was considered to proceed through surface-initiated spinodal decomposition in the cubic (NaCl) structure $Ti_{1-x}Al_xN$ lattice [9]. It has been shown that at the same composition of the TiAlN films the fraction of the w-AlN developing during the film growth depends on the parameters (e.g. on the bias voltage and deposition geometry [10], on the energy and momentum of metal ions incident at the growing film [11]). Most publications report on the formation of w-AlN phase, but fcc-AlN phase with epitaxial relation to the majority fcc-TiN phase has been also observed at Ti/Al = 2.7 ratio [12]. The fcc-AlN phase of well detectable fraction has been identified in the heat treated $Ti_{0.37}Al_{0.63}$ N films [13].

In the present paper we report the results of the structure analysis of selected $(Ti_{1-x}Al_x)_{1-y}Y_yN$ samples of the series of films reported in Ref. [7]) with mixed c-TiN and w-AlN structure and crossover in the c-TiN texture. We intend to collect the basic characteristics of the structure, necessary to identify the fundamental phenomena of structure formation, operating during the structure evolution and their pathway in dependence of the deposition parameters [14,15]. First of all we intended to understand in which stage of structure evolution and by which mechanism are the phases developing. Are they developing by primary nucleation on the substrate, by delayed nucleation related to the surface kinetic segregation or by surface/bulk spinodal decomposition? Furthermore, depositing the films at a temperature related to zone T of the structure zone diagram, how far the structure evolution is controlled by the competitive growth of the crystals of the fcc and wurtzite phases having various orientations [16].

2. Experimental details

The $(Ti_{1-x}Al_x)_{1-y}Y_yN$ films were prepared at 500 °C on ⟨001⟩ oriented Si single crystal substrates covered by natural oxide both by direct current magnetron sputtering (DC-MS) and by pulsed DC-MS in a modified Leybold Z-400 deposition system at the parameters described in details in Ref. [7]. With the target–substrate arrangement used in this facility (see Fig. 1 in [7]) only a small fraction of the vapour flux from the target section (directly below) arrives perpendicularly on the substrate, but the majority of vapour species is impinging at a certain angle with respect to the target–substrate axis. Therefore, tilted growth towards the vapour flux should be expected due to the oblique incident angles of the majority of the impinging metal species [17–19].

The microstructure of the films was investigated by X-ray diffraction (XRD) and by transmission electron microscopy techniques. For XRD analysis a Bruker AXS D8 Discover diffractometer equipped with Göbel-mirror and a 2D position sensitive (GADDS) detector system with Cu Kα radiation was used [20]. The intensity was acquired at four detector positions at nominal 2θ angles of 20°, 40°, 60° and 80°, covering the range of about 7°–93°, while the samples were positioned at θ = 10°, 20°, 30° and 40°, respectively. In the present diffraction patterns the Si 400 reflection is not shown because the measurements have been carried out at sample position θ = 30° and not at θ = 34.56°. For texture investigations, 2D diffraction patterns were acquired at the corresponding θ and 2θ angles and two or three different tilt (χ) angles. Sets of diffraction patterns at different φ rotational angles around the sample normal from 0° to 360° with 5° or 10° steps were recorded. Pole figures were constructed from these patterns by the GADDS software integrating the reflected intensity in a narrow 2θ window around the reflection of interest at each χ and φ positions (see details in [21]). Pole figures are displayed in stereographic projection, the diffraction vector is normal to the sample surface in the middle of the circles and is parallel to that at the edges.

The conventional transmission electron microscopic (TEM) and selected area electron diffraction (SAED) investigations of the cross sectional (X-TEM) and plane-view specimens were carried out in a PHILIPS CM20 transmission electron microscope equipped with a Ge-detector NORAN EDX analyser at 200 kV. The high resolution TEM investigations were carried out in a 300 kV JEOL 3010 transmission electron microscope.

The specimens for cross sectional (X-TEM) and plane-view transmission electron microscope investigations were prepared by mechanical and ion beam thinning techniques described in details in Ref. [7]. Since in our deposition facility tilted growth of columns towards the normal of the cathode was expected, the mechanical cutting of X-TEM specimens were taken from the radial axes of the samples as indicated in Figs. 1 and 7 of [7]. A special thinning technique was used to prepare plane-view specimens including the thickness range of nearly 0.2 μm of the film at the substrate [22]. This specimen made it possible to analyse the changes of the microstructure along the thickness on fine scale and to discover the variation of the phase composition and texture in the first and most decisive stages of the structure evolution.

3. Results and discussion

Results published in our previous paper [7] presented an overview on the variation of the phases, morphology and texture of the $(Ti_{1-x}Al_x)_{1-y}Y_yN$ alloy films in dependence of the Al content related to the range of the two-phase structure. In these experiments at Ti/Al ≥ 0.88 the films exhibited single phase c-TiN columnar structure with ⟨001⟩ fibre texture nearly parallel to the substrate surface normal (see Fig. 9 in [7]). In the composition range of 0.72 ≤ Ti/Al < 0.88 beside the ⟨001⟩c-TiN texture the w-AlN phase with ⟨0001⟩ texture showed up together with the <111> texture of the c-TiN phase (see Fig. 5 in [7]). The ⟨0001⟩ texture axis of the w-AlN and the <111> texture axis of the c-TiN were parallel and tilted to the direction of the vapour beam. The crystals of the two phases exhibited epitaxial relation $\{111\}_{TiN}\langle 110\rangle_{TiN}//\{0001\}_{AlN}\langle 11\text{-}20\rangle_{AlN}$. At the same time the ⟨001⟩c-TiN texture disappeared at a given thickness indicating the occurrence of a crossover in the c-TiN texture. This thickness varied both with the Al content and with the kind of applied sputtering method (DC-MS or pulsed DC-MS, see Figs. 4 and 6 in [7]). At the same ratio Ti/Al = 0.72 the crossover thickness was around 0.6 μm in the film deposited by pulsed DC-MS (the 5th sample in Table 1 in [7]), while it was very near to the substrate and even hardly detectable in the film deposited by DC-MS (the 1st sample in Table 1 in [7]).

In the following the structure and chemistry of the selected three films of the series of samples reported in [7] will be described and discussed: sample ***A*** with Ti/Al = 1 (prepared by DC_MS, the 3rd sample

in Table 1 of [7]), sample ***B*** with Ti/Al = 0.72 (prepared by pulsed DC-MS, the 5th sample in Table 1 of [7]), and sample ***C*** with Ti/Al = 0.72 (prepared by DC-MS, the 1st sample in Table 1 of [7]). Sample ***A*** had only the ⟨001⟩ cubic c-Ti(AlN) texture. In sample ***B*** the crossover in the c-TiN texture showed up at around 0.6 μm thickness. This sample made it possible to analyse the variation of the texture including the crossover with thickness on cross sectional specimen. In sample ***C*** the dominance of ⟨0001⟩ w-AlN//<111> c-TiN texture was detected already at around 0.1 μm thickness. Therefore sample ***C*** was especially suitable to investigate the structure developed in the first stages of film growth on fine thickness scale in plane-view specimen.

3.1. Structure of sample ***A***: $Ti_{0.49}Al_{0.49}Y_{0.02}N$ alloy film prepared by DC-MS (Ti/Al = 1)

3.1.1. X-ray diffraction analysis

The XRD spectrum A of the film shown in Fig. 1 corresponds to the diffraction pattern of cubic structure, space group Fm3m. Beyond the strong 200 peak, the spectrum contains also the 111, 220, 311 and 222 peaks of lower intensity indicating that, beside the pronounced ⟨001⟩ texture, randomly oriented crystals are also present in the film. The well-defined diffraction lines are between the diffraction lines of the unstressed c-TiN (JCPDS card number 38-1420) and c-AlN (JCPDS card number 25-1495) structures (positions of their reflections are marked). Only traces of c-AlN or w-AlN reflections [12,23,24] can be detected among the peaks. These indicate that the majority phase constituting the film is the cubic solid solution TiAlN phase with lattice parameters of 0.421 nm, 0.414 nm, 0.418 nm, 0.415 nm and 0.4155 nm calculated from the lattice spacings d(200), d(111), d(220), d(311) and d(222), respectively. The average of these values (0.4167 nm) agrees well with the value expected from Vegard's rule (0.417 nm) as determined in [25,26]. The pole figure taken by the 002 reflection (not shown) proved that the axis of the ⟨001⟩ texture is perpendicular to the substrate surface plane.

3.1.2. TEM and SAED analysis

The cross sectional bright field (BF) and dark field (DF) images of the film together with the SAED pattern taken from the whole cross section of the film including also the reflections of the Si substrate are shown in Fig. 2. The SAED pattern confirms the ⟨001⟩c-TiN texture with axis perpendicular to the Si substrate surface (marked by the Si 200 diffraction spot). The film is constituted of V-shaped columnar crystals with axis perpendicular to the substrate surface plane, indicating that this columnar structure and texture have been developed by competitive growth of crystals.

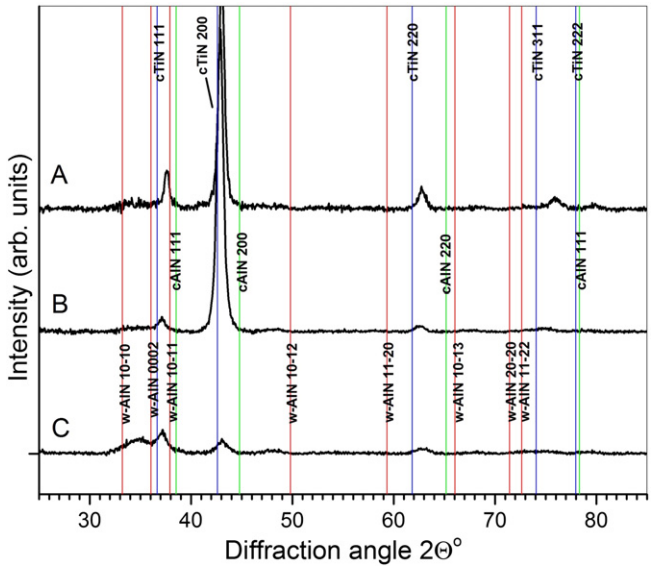

Fig. 1. The XRD spectra of $(Ti_{1-x}Al_x)_{1-y}Y_yN$ films of Ti/Al ratio: Ti/Al = 1 (***A*** sample, prepared by DC-MS), Ti/Al = 0.72 (***B*** sample, prepared by pulsed DC-MS) and Ti/Al = 0.72 (***C*** sample, prepared by DC-MS). Sites of reflections of unstressed c-TiN (JCPDS card number 38-1420), c-AlN (JCPDS card number 25-1495) and w-AlN (JCPDS card number 25-1133) are marked.

3.2. Structure of sample ***B***: $Ti_{0.41}Al_{0.57}Y_{0.02}N$ alloy film prepared by pulsed DC-MS (Ti/Al = 0.72)

3.2.1. X-ray diffraction analysis

In the knowledge that the columns are off surface normal in the upper part of the film (see later in Fig. 4), the 2θ diffraction plot shown in Fig. 1B represents only the structure of the first thickness range, in which the columns are perpendicular to the substrate surface plane. This XRD plot corresponds also to the diffraction plot of cubic structure, space group Fm3m. The very strong 002 diffraction line indicates the dominance of the ⟨001⟩c-TiN texture which will be unambiguously confirmed by the SAED investigation (see later in Figs. 4 and 5). The position and shape of the diffraction lines could correspond also to a solid solution TiAlN phase as discussed in case of sample ***A***. Pole figures can provide more detailed information on the whole structure of the film (Fig. 3(a), (b) and (c)). The bright spot in the centre of the pole figure taken by c-TiN 200 reflection (Fig. 3(a)) confirms the existence of c-TiN⟨001⟩ texture with axis perpendicular to the substrate surface as shown in the 2θ diffraction plot in Fig. 1 (spectrum B). The bright spot in the pole figure of Fig. 3(b)) taken by the c-TiN 111 reflection shows the presence of the <111> texture, a second texture of the c-TiN phase. However, the axis of the <111> texture is tilted about 20° off normal direction. The central bright diffraction ring is due to the 111 c-TiN reflections of the ⟨001⟩ oriented c-TiN crystals. In Fig. 3(c) the diffraction spot with low intensity in the direction of 20° off normal (in the same direction as that of the c-TiN⟨111⟩ direction in Fig. 3(b) taken by the w-AlN 0002 reflection demonstrates the existence of the w-AlN⟨0001⟩ texture. The bright central ring on this plot probably originates from the c-TiN 111 reflection which is close to the w-AlN 0002 reflection. In reality, it is very probable that the c-TiN 111 and w-AlN 0002 reflection contributions overlap in the corresponding pole figures due to the very small difference in their lattice spacing (0.245 nm and 0.249 nm respectively), which could be further reduced by the formation of solid solutions.

3.2.2. TEM analysis

The cross sectional TEM images of sample ***B*** shown in Fig. 4 demonstrate that the film has V-shaped columnar structure and is composed of two, well distinguishable thickness ranges. In the first range, grown on the substrate, most of the V-shaped columns are nearly parallel to the substrate surface normal (~5° off), while in the upper part of the film the columns are more tilted (~20° off). The SAED pattern (Fig. 4(d)) taken from an area including both the substrate and the whole cross section of the film indicates the coexistence of the c-TiN⟨001⟩ and the tilted w-AlN⟨0001⟩//c-TiN⟨111⟩ textures, in which the close packed planes of the c-TiN and w-AlN crystals are parallel. The axis of the c-TiN⟨001⟩ texture (indicated by the stronger arch on the c-TiN 200 ring) is nearly parallel (~5° off) to the substrate surface normal marked by the Si 200 reflection. The texture axes of the w-AlN⟨0002⟩//c-TiN ⟨111⟩ textures are in accordance with the tilt of the morphology. The DF-TEM image (Fig. 4(c)) taken by the c-TiN 200 reflection demonstrates that the c-TiN<001> texture with texture axis nearly parallel to the substrate surface normal corresponds to the first thickness range, where the columns are also nearly parallel to the substrate surface normal. The V-shaped morphology of the ⟨001⟩ oriented TiN crystals (marked by A in Fig. 4(c)) indicates that the c-TiN⟨001⟩ texture is developed by competitive growth. The DF-TEM image taken by the c-TiN 111 and w-AlN 0002 reflections shows that the TiN and AlN crystals with parallel w-AlN⟨0001⟩//c-TiN⟨111⟩ orientation have absolute dominance

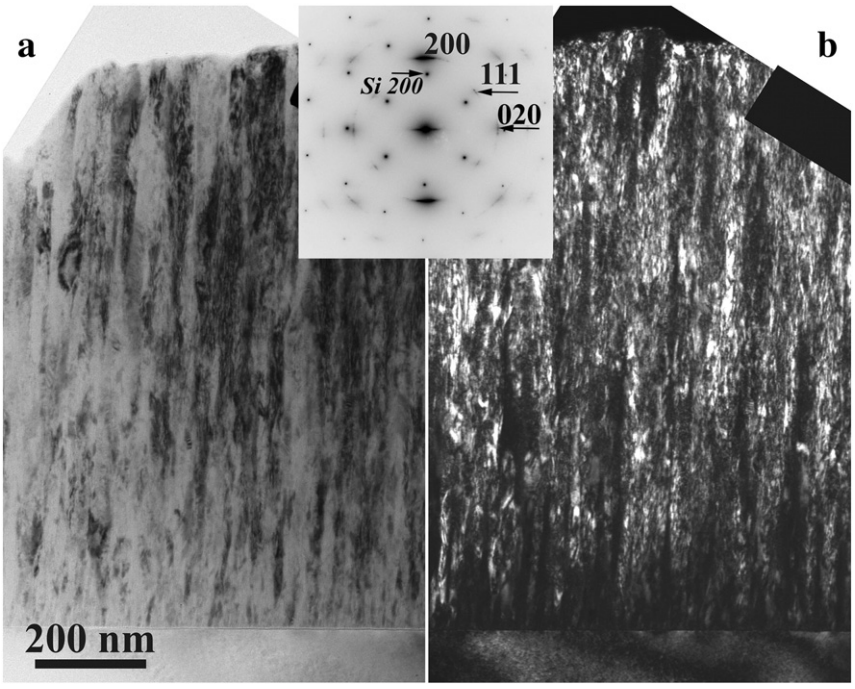

Fig. 2. Bright field (BF) and dark field (DF) TEM images of sample A (Ti/Al = 1). The SAED pattern shows the single cubic phase with sharp ⟨001⟩ texture perpendicular to the substrate. The single crystal diffraction spots are due to the Si single crystal substrate in the [011] zone axis.

in the upper thickness range of the film (Fig. 4(b)). Thanks to the oblique deposition, the thickness ranges in which either the c-TiN ⟨001⟩ or the tilted w-AlN⟨0001⟩//c-<111> textures are present with high intensity (see SAED pattern of Fig. 4(c)), can be identified also in the morphology. Namely the columns become more tilted also at the thickness where the crossover between the c-TiN⟨001⟩ and c-TiN⟨111⟩ texture occurs. This thickness is about 0.6 μm in sample ***B***.

The distribution of textures along film thickness has been determined also by SAED patterns (Fig. 5). SAED pattern of Fig. 5(b) taken on the thickness range at the substrate contains continuous diffraction rings of the c-TiN phase with intensive arcs on the 002 diffraction circle nearly in the direction of the substrate surface normal (~5° off). This demonstrates that beside randomly oriented TiN crystals, there are c-TiN crystals with ⟨001⟩ preferred orientation. In this SAED pattern week and diffuse arches of the w-AlN 0002 together with the arches of the c-TiN 111 diffraction rings can be identified near to the direction of the substrate surface normal (~5° off). The SAED pattern of Fig. 5(d), taken from the upper thickness range of the film shows only strong and parallel w-AlN 0002 and c-TiN 111 reflections at about 20° out of the substrate surface normal. This clearly proves that in this thickness range only c-TiN and w-AlN crystals with parallel orientation were grown. The arches on the other diffraction rings are related also these crystals. The SAED pattern of Fig. 5(c), taken on the central thickness range of the film, contains continuous diffraction rings of c-TiN and superposed intensive arches due to the c-TiN⟨001⟩ and the tilted w-AlN <0001>//c-TiN⟨111⟩ textures. Directions of the texture axes correspond

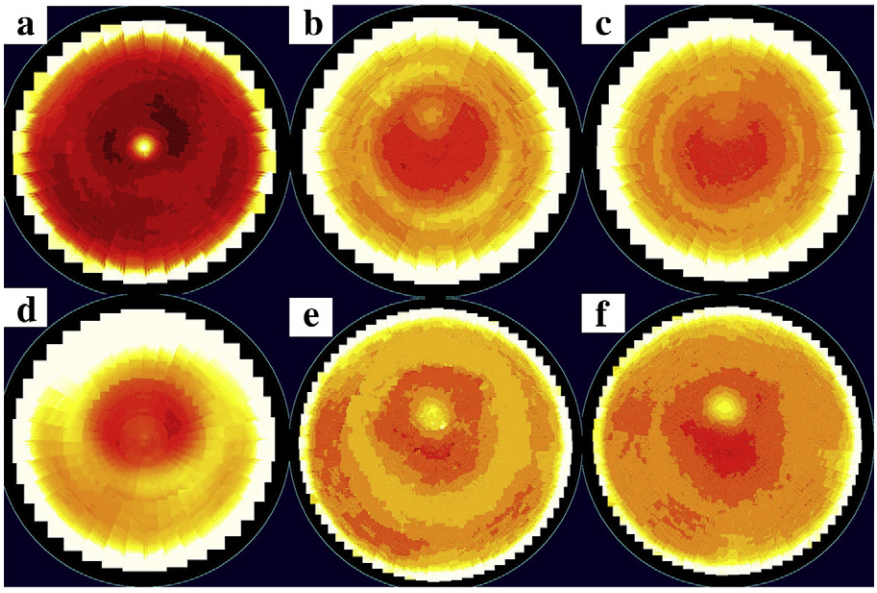

Fig. 3. Pole figure plots of samples; 1st line: sample ***B*** (Ti/Al = 0.72, prepared by pulsed DC-MS), 2nd line: sample ***C*** (Ti/Al = 0.72, prepared by DC-MS); (a) and (d) are taken by c-TiN 002, (b) and (e) are taken by c-TiN 111, and (c) and (f) are taken by w-AlN 0002 reflections.

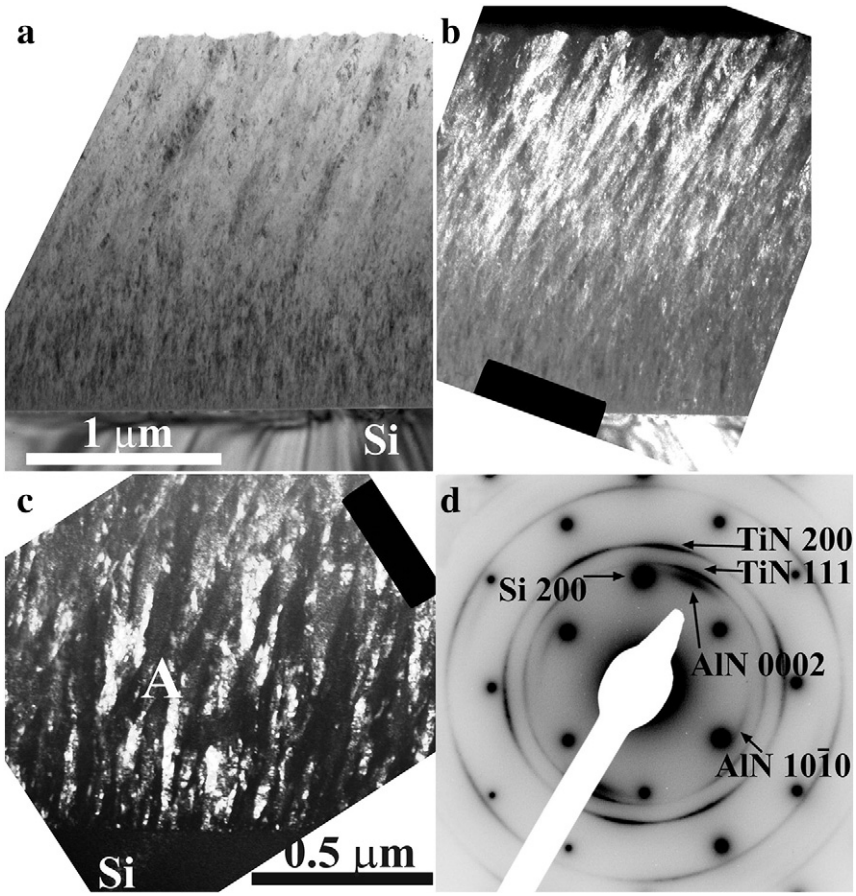

Fig. 4. BF TEM image of the $Ti_{0.41}Al_{0.57}Y_{0.02}N$ alloy film prepared by pulsed DC-MS (sample ***B***). SAED pattern (d) is taken from an area including the substrate and the whole cross section of the film, the spotty pattern is due to the Si single crystal with [011] zone axis parallel to the electron beam; the substrate surface normal is marked by the 200 Si reflection; b) DF TEM image taken by the w-AlN 0002 and c-TiN 111 reflections; c) DF TEM image taken by the c-TiN 200 reflection; A marks a V-shaped c-TiN crystal; SAED pattern is adjusted to the substrate surface normal.

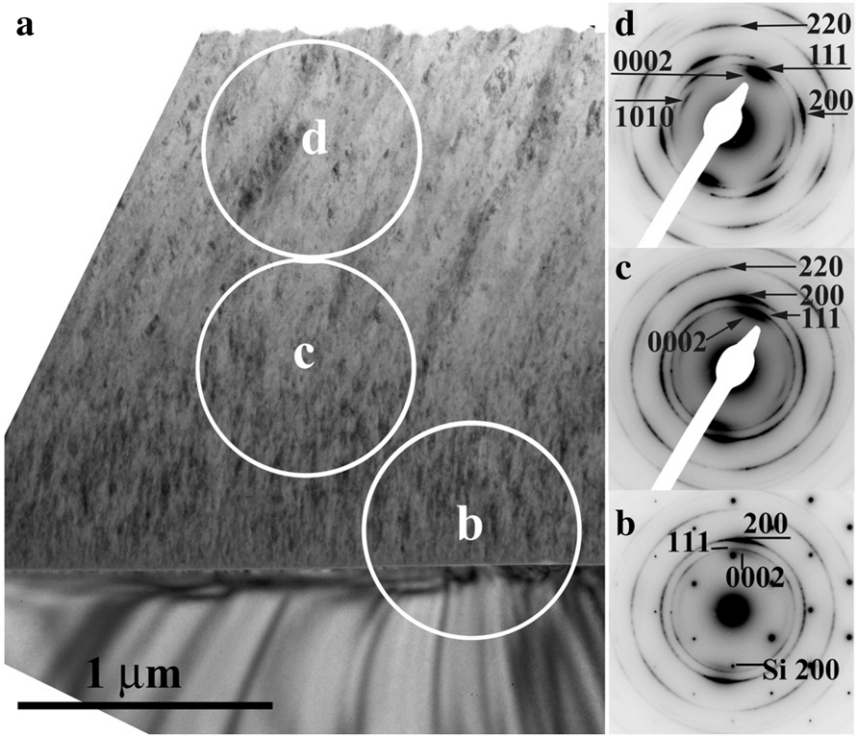

Fig. 5. BF TEM image and SAED patterns taken at the different thickness ranges of the $Ti_{0.41}Al_{0.57}Y_{0.02}N$ alloy film prepared by DC-MS (sample B); the spotty pattern is due to the Si single crystal with [011] zone axis parallel to the electron beam. SAED patterns are adjusted to the substrate surface normal.

to those of the lower and upper thickness ranges described above. This diffraction pattern demonstrates the coexistence of the c-TiN⟨001⟩ and the tilted w-AlN⟨0001⟩//c-TiN⟨111⟩ textures, but randomly oriented crystals of the c-TiN phase are still present.

These results indicate that both phases are present in this film from the very beginning of film growth but with changing quantity and orientation relations. In the first growth stage the c-TiN with developing ⟨001⟩ texture is the majority phase and dominates the structure. However, at the same composition of the condensing vapour beam, the fraction of the w-AlN phase increases with thickness, developing simultaneously the tilted w-AlN⟨0001⟩//c-TiN⟨111⟩ texture. From the central thickness range the ⟨001⟩ oriented c-TiN crystals disappear and the structure is constituted of nano-crystalline w-AlN and c-TiN phases with parallel w-AlN⟨0001⟩//c-TiN⟨111⟩ orientations.

3.3. Structure of sample *C*: $Ti_{0.41}Al_{0.57}Y_{0.02}N$ alloy film prepared by DC-MS (Ti/Al = 0.72)

3.3.1. X-ray diffraction analysis

In this film the columns are also off surface normal in the upper part of the film (Fig. 6), therefore the 2θ diffraction plot shown in Fig. 1 (spectrum C) represents only the structure of the first thickness range, in which the columns are perpendicular to the substrate surface. Beside the weak and broad diffraction peaks, corresponding to the diffraction plot of the c-TiN structure, this XRD plot contains a weak and very broad diffraction peak between the markers of the w-AlN 10-10 and 0002 reflections. All of these indicate that very low quantities of both phases are present in the first thickness range, on one hand. On the other hand, the size of coherent scattering w-AlN domains has to be extremely low (in the 2–3 nm range). Information on the whole structure of the film is provided by the pole figures taken by the c-TiN 200 and 111, and by the w-AlN 0002 reflections shown in Fig. 3(d), (e) and (f). The pole figure plot taken by the c-TiN 200 reflection (Fig. 3(d)) contains a weak, diffuse spot about 5° off normal direction, indicating a weak ⟨001⟩ texture of the c-TiN. The pole figures in Fig. 3(e) and (f) show the presence of parallel c-TiN⟨111⟩ and w-AlN⟨0001⟩ textures, very similar to sample ***B*** shown in Fig. 3(b) and (c).

3.3.2. TEM analysis

The detailed structure analysis has been carried both on cross sectional and plane-view specimens. The BF X-TEM image of the film (Fig. 6) demonstrates the existence of the same thickness ranges with the characteristic columnar structures as described in case of sample ***B*** (Fig. 4). However, according to the onset of the tilting of the columns near to the substrate, the first thickness range at the substrate is much thinner and the crossover in the c-TiN texture (marked also by the tilting of the columns) sets in already at around 0.1 μm thickness. The columns are V-shaped indicating that the structure is developed by competitive crystal growth.

The SAED pattern taken from the whole cross section of the film (Fig. 6(c)) demonstrates that the w-AlN⟨0001⟩//c-TiN⟨111⟩ textures dominate in the structure. The rather diffuse nature of the diffraction rings and arches indicates, however, immediately that the film should have a unique structure. Namely, the effective size of crystals domains scattering the electrons coherently has to be in the nm range, though the structure is constituted of well developed (textured) columns

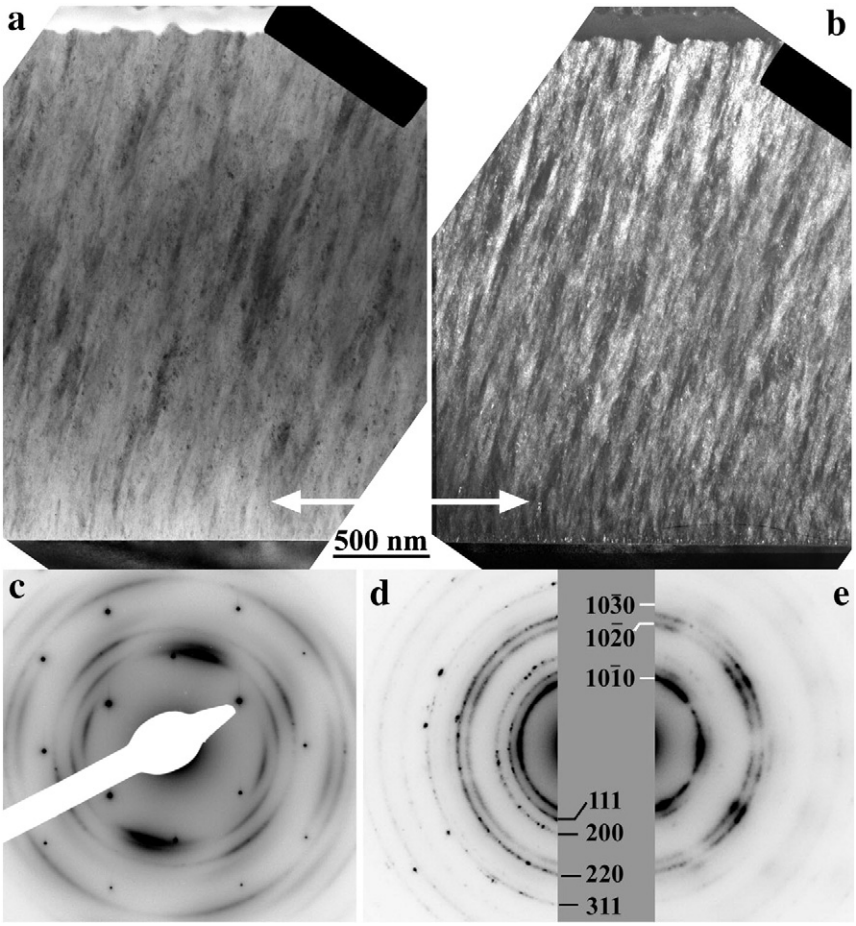

Fig. 6. BF (a) and DF (b) X-TEM images of the $Ti_{0.41}Al_{0.57}Y_{0.02}N$ alloy film prepared by DC-MS (sample ***C***); the DF image was taken by the c-TiN 111 and w-AlN 0002 reflections shown in (c); the crossover in the c-TiN texture is marked by a white arrow; (c) is the SAED pattern taken on an area including one part of the Si single crystal substrate and the whole cross section of the film; (d) and (e) show the SAED patterns of the plane-view specimens prepared from the thickness ranges at the substrate and at the upper part near to the surface of the film, respectively.

proceeding through the whole thickness of the film. Consequently the columns should have a substructure built up by c-TiN and w-AlN nanocrystals with strict orientation relations. In addition to that the diffraction rings of the SAED patterns of the plane-view specimens taken from the first thickness range at the substrate (Fig. 6(d)) and from the upper part (Fig. 6(e)) have different characters. In the SAED pattern of the first thickness range (Fig. 6(d)) discrete diffraction spots of larger single crystals are superposed on the continuous diffuse background of the 111 and 200 diffraction rings of c-TiN while the diffraction rings of the w-AlN crystals are continuous and diffuse. In contrast, the diffraction rings of both c-TiN and w-AlN in the SAED pattern from the upper thickness range (Fig. 6(e)) are diffused though the diameter of the columns is large. The diffused character of the w-AlN diffraction rings in both diffraction patterns indicates that the dimension of w-AlN crystals is in the nm size in both thickness ranges. However, the character of the c-TiN diffraction rings indicates that both nm size and larger TiN crystals are present in the first thickness range. In the second thickness range, only nm size TiN crystals are present like the w-AlN ones.

The key issue is now to discover the variation of the structure, especially the orientation of crystals, with the thickness on a fine thickness scale in the first thickness range at the substrate and the very unique substructure of the well-developed columns in the upper thickness range where the w-AlN⟨0001⟩//c-TiN⟨111⟩ textures of nm size crystals dominate.

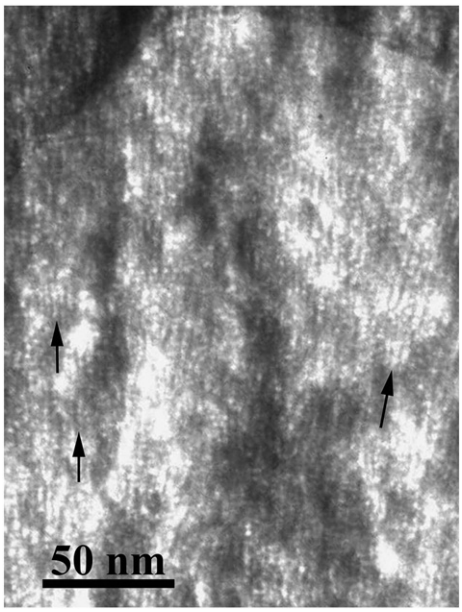

Fig. 8. The "pearl-necklace"-like fibre substructure of the columns shown in Fig. 6(b). Dark field TEM image taken by the w-AlN 0002 and c-TiN 111 reflections.

3.3.3. The structure of the film in the upper thickness range

In the upper thickness range of this film the columns are tilted (Fig. 6(a) and (b)) and preferentially orientated (Fig. 6(c)) in the cross section but they are of random azimuthal orientation (Fig. 6(e)). Fig. 7(a) and (b) show the phase contrast TEM images of the film in side and plane-view respectively. The column boundaries (marked by arrows) are well visible. The diameter of the columns is in the range of 100–200 nm. According to the phase contrast images the column boundaries are covered by a foreign phase which is possibly related to the contamination incorporated during deposition, or pores are present.

The existence of the nano-size substructure of the film anticipated from the SAED patterns of the X-TEM specimen is to be seen in the DF X-TEM images of Figs. 6(b) and 8 taken by the w-AlN 0002 and c-TiN 111 reflections. These images show that the nanocrystals constituting the columns are remarkably ordered forming also fibres that are arranged more or less parallel to each other and to the axis of the columns. At higher magnification (Fig. 8) the fibres manifest as lined-up distinct nanocrystals in the dark field TEM image. Indeed, sometimes they are "pearl necklace"-like features (marked by arrows) which is unique in nano-crystalline composites.

A representative cross-sectional HRTEM image (a) and its fast Fourier transform (FFT) pattern (c) are shown in Fig. 9. For comparison the conventional SAED pattern is also enclosed (Fig. 9(b)). The two patterns are the same, only the specimen was slightly tilted around the [10-30] axis during the HRTEM imaging. That is why the w-AlN 0002 reflections are weak and the corresponding c-TiN 111 ones are hard to recognize (Fig. 9(c). In Fig. 9(b) the coexistence of the w-AlN⟨0001⟩//c-TiN⟨111⟩ orientations is also clearly shown.

The spatial distribution and size of the coexisting domains of the c-TiN and w-AlN phases can be identified in the HRTEM image shown in Fig. 10(a). FFT of the HRTEM image proves the presence of c-TiN and w-AlN phases. The marks in the HRTEM image indicate the c-TiN 200 and the w-AlN 10-10 lattice fringes as they are alternately stacked on top of each other with a 3–5 nm period. In Fig. 10(b) and (c) the HRTEM image with two pairs of alternating wurtzite and fcc nanocrystals and the corresponding FFT pattern of the same area are shown. The result of Fourier filtering of the image in Fig. 10(b) is shown in Fig. 10(d) and (e). Fig. 10(d) is composed only by the reflections of the hcp, while Fig. 10(e) with the reflections of the fcc phase. It is clearly seen that the lattice fringes in HRTEM images of

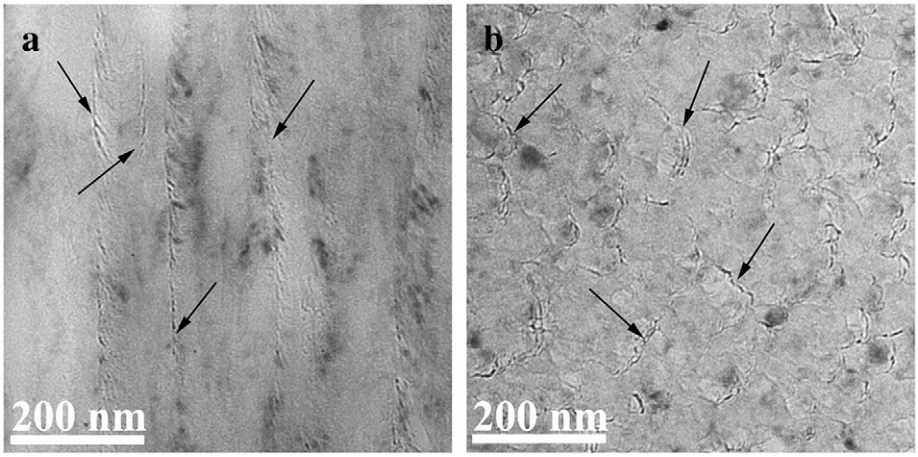

Fig. 7. Phase contrast X-TEM (a) and plane-view (b) TEM images of the $Ti_{0.41}Al_{0.57}Y_{0.02}N$ alloy film prepared by DC-MS (sample ***C***). Column boundaries are marked by arrows.

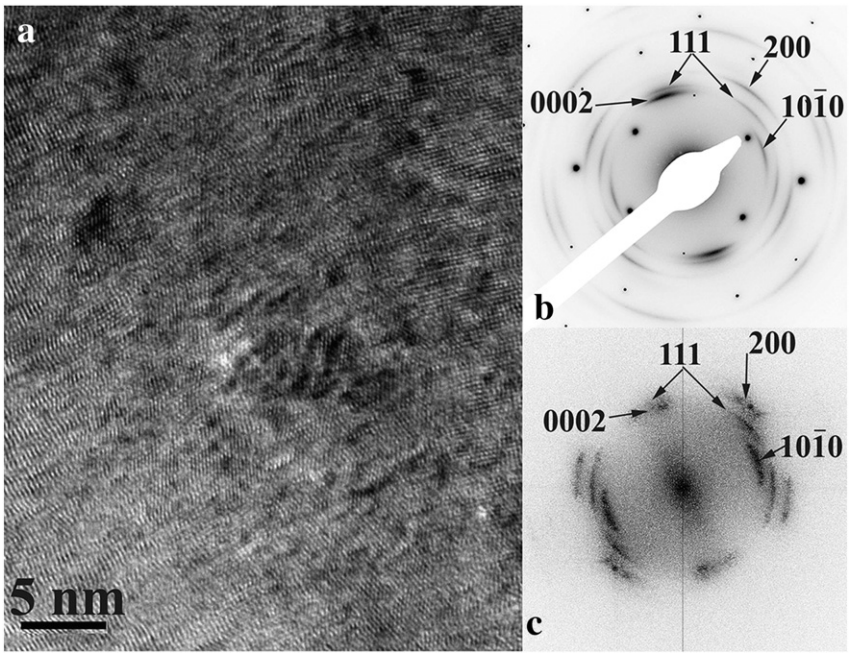

Fig. 9. Cross-sectional HRTEM image (a) and FFT (c) of the $Ti_{0.41}Al_{0.57}Y_{0.02}N$ alloy film prepared by DC-MS (sample ***C***) and (b) is the corresponding conventional SAED pattern.

Fig. 10(d) and (e) are complementary, proving the alternate stacking of w-AlN and c-TiN phases. This gives rise to the "pearl-necklace" structure shown in Fig. 8.

For the interpretation of the structure of the boundaries and the identification of the appearing lattices (phases) structural models were built and image simulation on these models was performed by the JEMS program [27]. Matching of the computed and observed HRTEM images (Fig. 11) proves that the growing supersaturated phase (it will be shown later that it is the w-Al(Ti)N) is decomposed into c-Ti rich and w-Al rich nitrides. These phases differ only on their stacking sequence of the close packed planes, so the separation could be started by spinodal decomposition without nucleation [28,29]. The occurrence of the fcc phase, however, points to the fact that spinodal decomposition might have developed to the state, close to nucleation. The coherency of the wurtzite–fcc interfaces on the close packed planes is maintained, but in other directions it should be replaced by (semi-coherent) phase boundaries.

TEM analysis of the plane-view specimens provides further information on the morphology, orientation and distribution of the c-TiN and w-AlN nanocrystals. The dark field TEM image of the plane-view specimen taken by the w-AlN 10-10 reflection indicates that the wurtzite nanocrystals with nearly identical in-plane orientation are grouped into domains (spotty bright domains in Fig. 12(a)). The size of these domains indicates that they correspond to the cross sections of the individual columns shown in Fig. 7(a). The SAED pattern taken from larger area (Fig. 12(b)) demonstrates the random in-plane (azimuthal) orientation of the individual columns. The SAED pattern of Fig. 12(c) taken from the encircled area shows that the c-TiN and w-AlN nanocrystals within the columns have parallel in-plane orientation with c-TiN⟨220⟩//w-AlN⟨11-20⟩, i.e. they are in epitaxial relation with $\{111\}_{TiN}\langle 110\rangle_{TiN}//\{0001\}_{AlN}\langle 11\text{-}20\rangle_{AlN}$.

Fig. 13 presents the plane view HRTEM image of the film including a column boundary (marked with dashed line) between A and B columns. According to the FFTs taken on columns A and B, the nanocrystals are

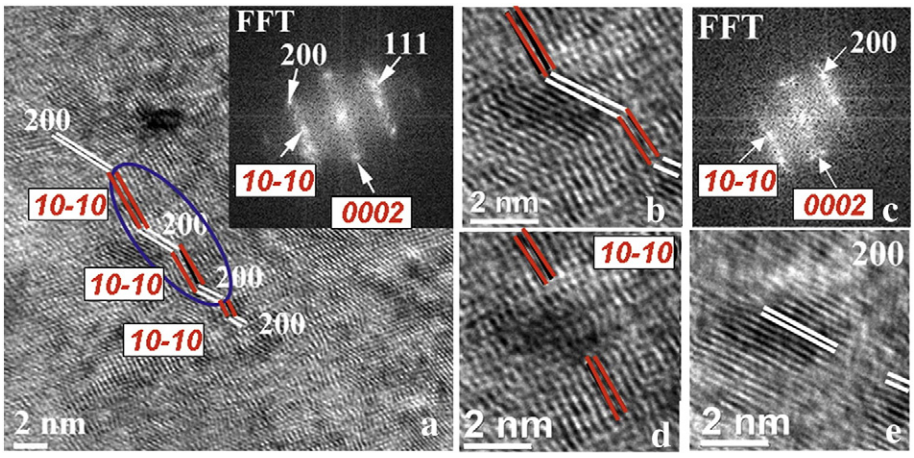

Fig. 10. Sample ***C***: HRTEM image (a) with inserted FFT pattern and (b) enlarged detail of the HRTEM image with two pairs of alternately stacked wurzite and fcc nanocrystals and corresponding FFT pattern. (c), (d) and (e) are filtered HRTEM images taken with the hcp and fcc reflections, respectively.

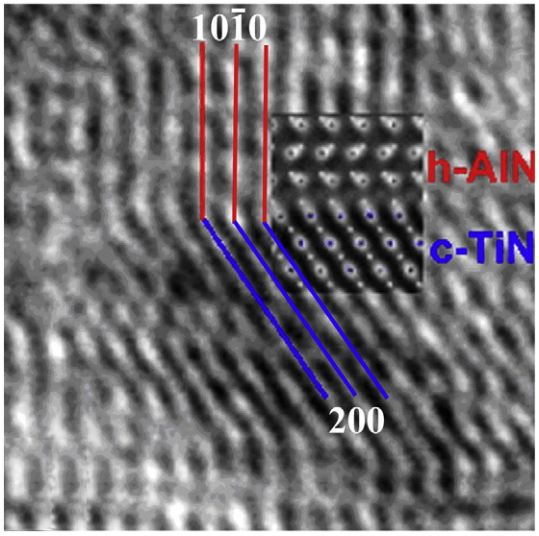

Fig. 11. Sample ***C***: HRTEM micrograph showing the plane matching of w-AlN (10-10) and c-TiN (200) lattice planes. The nanocrystals could develop by spinodal decomposition in the columns of supersaturated w-AlTiN solid solution phase during the growth of the film. The insert shows the corresponding atomic arrangement. In the atomic columns larger dots represent the Al and Ti atoms, accordingly. The small dots represent N atoms. The simulated image of the atomic interface model is calculated for 60 nm defocus and 6 nm layer thicknesses.

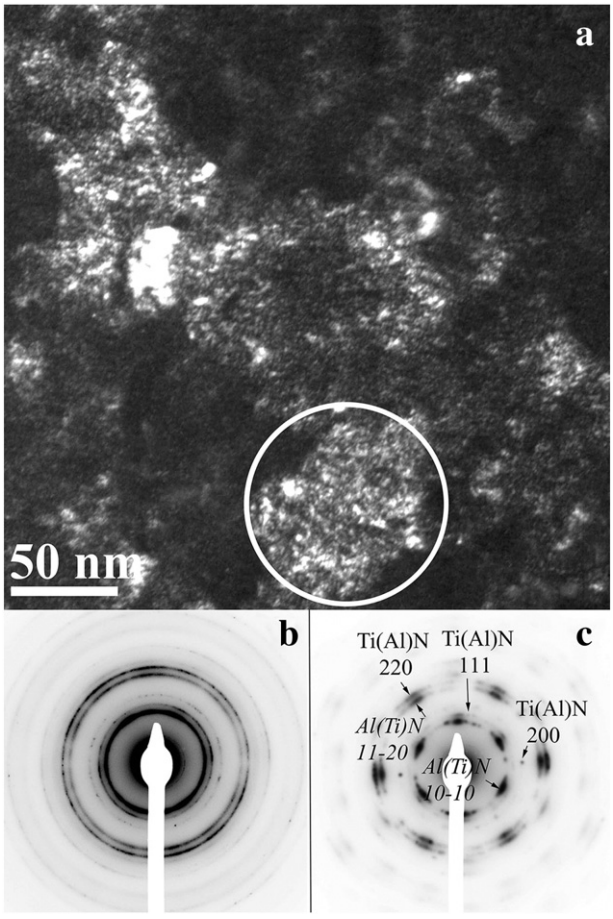

Fig. 12. Sample ***C***: plane-view DF TEM image (a) taken by the w-AlN 10-10 reflection; (b) is the electron diffraction pattern of the film; and (c) is the SAED pattern taken from the area encircled in (a).

identically oriented within the columns, while the columns exhibit a 15° azimuthal misorientation as measured in the FFT taken from the area including both columns.

The HRTEM image shown in Fig. 14 illustrates c-TiN crystallites with [001] orientation ({200} lattice planes are imaged) and possibly with [111] orientation (one set of {220} lattice planes are imaged) within the w-AlN lattice of an [0001] oriented column, illustrating also the two phase structure of individual columns.

3.3.4. Structure of the film in the lower thickness range (above the substrate)

Because the film was deposited in zone T and no restructuring of the developed structure could take place, the steps of structure evolution leading from nucleation to the structure of the upper part are preserved. By this way, the knowledge of the variation of the structure in this thickness range on very fine thickness scale could make possible to reconstruct the pathway of structure evolution from the nucleation across the crossover in the texture of the c-TiN phase to the onset of the oriented growth regime with the unique nano-composite structure described above.

In this thickness range the most decisive structure investigation has been carried out on plane-view specimens prepared by a specific thinning technique [22]. These specimens included a thickness range of about 0.2 μm at the substrate in which the various plane-view areas belonged to different thicknesses ranges. Though the exact location of the actual investigated area along the thickness could not be unambiguously identified, one could recognize at least the areas located successively farther and farther from the Si single crystal substrate along the film thickness. The most important information on existing phases and orientation relations of their crystals are presented by the SAED patterns taken from the areas of thickness sections at increasing distances from the substrate (Fig. 15). These SAED patterns were taken at two positions (orientations) of the plane-view specimen. One kind of patterns (shown in the first line) was taken at normal electron beam incidence, while the patterns shown in the second line were taken at tilted specimen position. Taking SAED patterns at tilted specimen position is an important benefit, because the arching of the diffraction rings indicates immediately if the crystals of a phase or a part of them are with preferred orientation (texture) [30].

The SAED patterns of Fig. 15(a) and (e) represent the structure grown in the very first stage of film deposition on the oxidised Si substrate, while those of Fig. 15(b) and (f) are taken from the next area with higher film thickness also on the substrate. In the patterns of Fig. 15(a) and (e) all diffraction rings of c-TiN and w-AlN phases are present together with the diffraction spots of Si single crystal. In case of (a) the direction of the electron beam was parallel with the substrate surface normal (Si [001]), while in case of (e) it was parallel with the Si [103], i.e. the specimen was tilted ~20°. Any arching of the diffraction rings of both phases is hardly detectable in Fig. 15(e). That means that crystals of both phases nucleated with random orientation on the substrate. In Fig. 15(b) and (f) all diffraction rings of both phases are also present but with stronger intensity. This indicates that the film is thicker than in case of Fig. 15(a) and (e). However, in Fig. 15(f) a weak arching can be identified already on the 10-10 and 11-20 w-AlN diffraction rings along the tilting axis, while still no arching is detectable on the c-TiN diffraction rings. This indicates that with increasing film thickness some part of the growing w-AlN crystal is already in the preferred ⟨0001⟩ orientation in contrast to the c-TiN phase.

The lack of diffraction spots of the substrate Si crystal in Fig. 15(c) and (g) indicates that this area was located farther from the substrate and does not include the very first thickness range near to the substrate. According to Fig. 15(g) the arching of the 10-10 and 11-20 w-AlN diffraction rings along the tilting axis is stronger but the continuous background of these rings is still present with low intensity. That means that larger part of the w-AlN phase is now accumulated in the ⟨0001⟩ oriented crystals, indicating that the ⟨0001⟩w-AlN texture

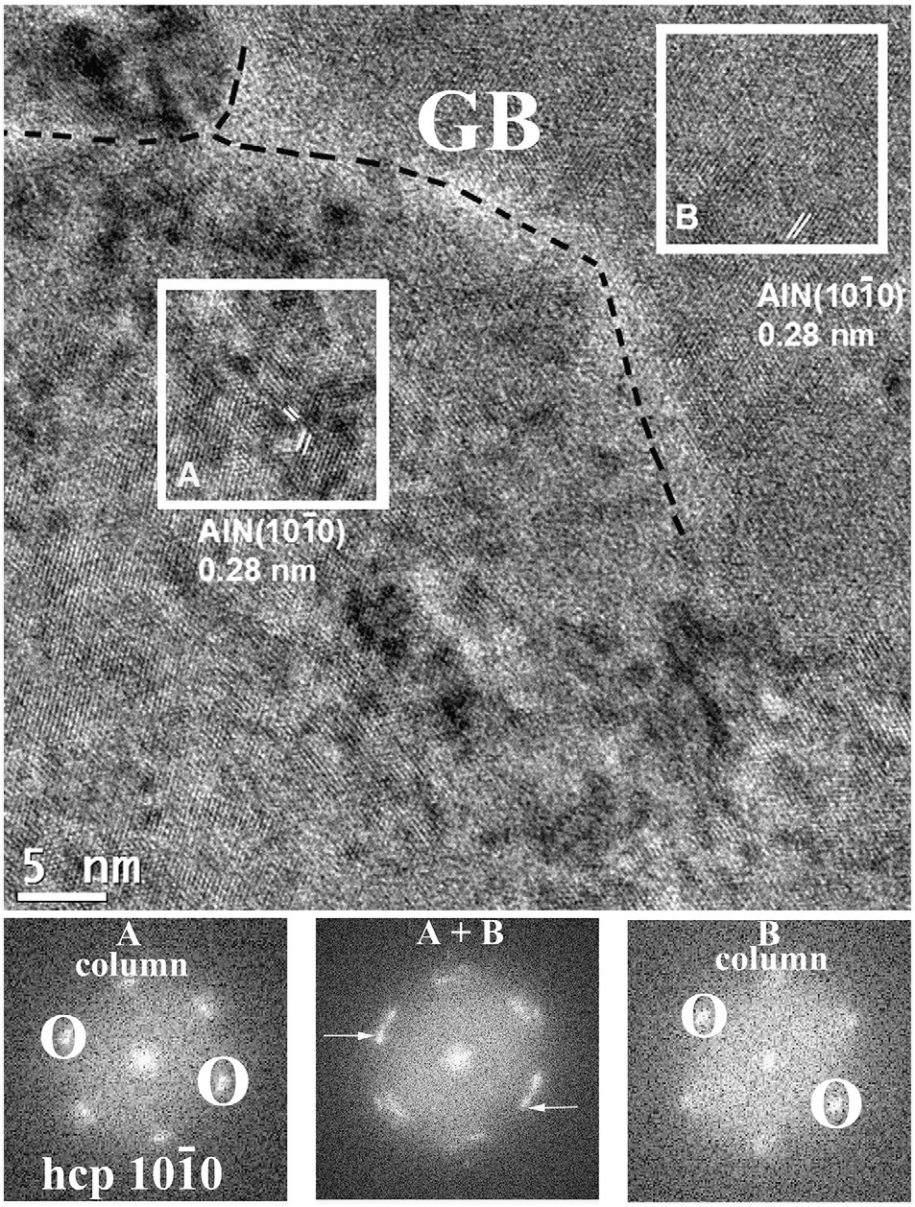

Fig. 13. Sample ***C:*** HRTEM image of an area of the plane-view specimen including the boundary between neighbour columns A and B; the FFTs taken from columns A and B prove that the nanocrystals within the columns have azimuthal misorientation; the FFT taken from the two columns indicates 15° azimuthal misorientation of these columns.

started to develop. Simultaneously, arches are also detectable on the c-TiN diffraction rings. The arching is stronger on the 220 ring and these arches are strong in the direction of the arches on the 10-10 and 11-20 w-AlN diffraction rings along the tilting axis marked by the arrows. This arching of 220 ring points to the appearance of <111> oriented c-TiN crystals with axis parallel to the electron beam and to the texture axis of w-AlN crystals. Less pronounced arches are present on the continuous 111 and 200 c-TiN diffraction rings in the direction perpendicular to the tilting axis. Accordingly, the diffraction pattern taken at normal electron beam incidence is also changed. The intensity of the 111 and 200 diffraction rings of c-TiN strongly decreased while that of the 220 ring increased. All of these changes indicate that in the structure of the w-AlN phase now the ⟨0001⟩ texture started to dominate at this thickness, and a well detectable part of the c-TiN phase is present now in crystals with <111> orientation parallel to the preferentially oriented w-AlN crystals. That is, however, the w-AlN[0001]//c-TiN[111] parallel orientation characterising the upper part of the film as discussed in details before. The strong arches of the diffraction rings in the SAED pattern of Fig. 15(h) taken on the next area indicate that at this thickness the largest part of crystals of both phases are now oriented with the w-AlN[0001]//c-TiN[111] orientation relationship. Accordingly the SAED pattern of Fig. 15(h) includes only the 10-10 and 11-20 w-AlN and the 220 c-TiN diffraction rings of high intensity due to the w-AlN ⟨0001⟩ and the c-TiN⟨111⟩ textures.

The cross sectional HRTEM image taken at the Si single crystal substrate and film interface (Fig. 16) shows a V-shaped crystal, nucleated on the substrate. The lattice fringe image of this crystal and its FFT pattern shown in the inset is identical with those of columns constituting the upper thickness range of the film shown in Figs. 9 and 10. This confirms that the columns with the w-AlN and c-TiN nano-composite substructure winning the competitive growth and constituting the textured two phase $Ti_{0.41}Al_{0.57}Y_{0.02}N$ alloy film at higher film thicknesses are nucleated on the substrate.

4. Summary

Wahlström et al. [8] have shown that in case of $Ti_{1-x}Al_xN$ alloy films three composition zones can be identified which are due to

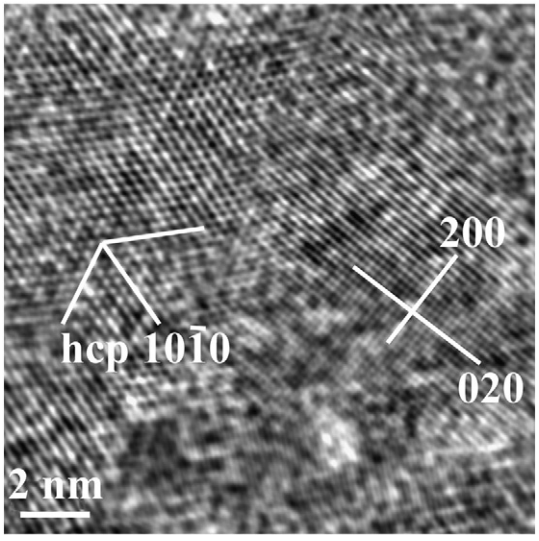

Fig. 14. Sample ***C***: HRTEM image of adjacent columns in the plane view specimen showing the lattice images of w-AlN in [0001] orientation and c-TiN in [001] orientation.

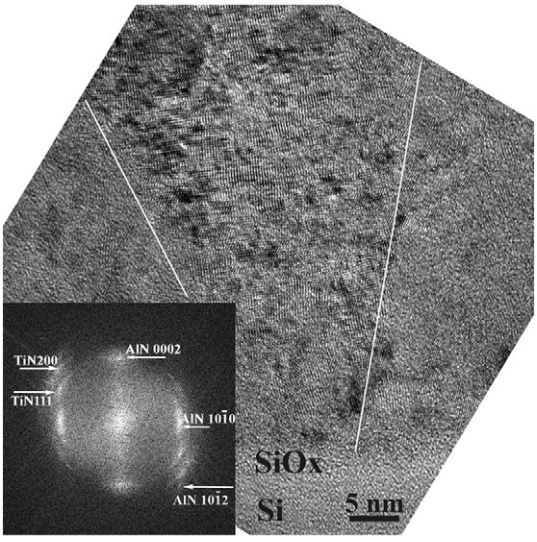

Fig. 16. Sample ***C***: cross sectional HRTEM image of the first thickness range at the substrate; the FFT pattern shows the parallel w-AlN[0001]//c-TiN[111] orientation of the nanocrystals constituting the V-shaped column.

regions of different phases. These composition zones could be signed as **S1**, with single (or majority) phase Al rich c-TiAlN solid solution phase, **TW**, with two phases, Al rich c-TiAlN and Ti rich w-AlTiN, and **S2**, with single (or majority) phase Ti rich w-AlTiN solid solution. Analysis of the present results anticipates that in case of $(Ti_{1-x}Al_x)_{1-y}Y_yN$ alloy films the TW composition zone could consist of two subzones, **TW1** and **TW2** which can be defined also by distinct structures when the films have grown to appropriate thickness (film thickness >1 μm). In the present experiments zone TW1 following zone S1 could be the 0.72 < Ti/Al < 0.88 composition range, which is characterised by two phases and three coexisting textures. Zone TW2 would have also the same two phases but only two textures.

In our experiments, due to the oblique deposition, the three textures in zone TW1 are the c-TiN⟨001⟩ texture with axis nearly perpendicular to the substrate surface, the c-TiN⟨111⟩ with off normal axis and the w-AlN⟨0001⟩ texture also with off normal axis. Moreover, the axes of c-TiN ⟨111⟩ and w-AlN⟨0001⟩ textures are parallel and the successively dominant c-TiN⟨001⟩ and <111> textures show an orientation crossover (Figs. 4, 5 and 6). It has been demonstrated that the development of this specific structure is related unambiguously to the simultaneous nucleation of the randomly oriented crystals of the c-TiN and w-AlN phases on the substrate (Fig. 15), as proposed for multi-component films [16]. The c-TiN crystals grow as columns of TiAlN solid solution phase. The w-AlN crystals grow as columns of supersaturated solid solution incorporating excess Ti species [16]. These excess species will form the c-TiN crystal domains most probably by surface spinodal decomposition [9]. These c-TiN crystal domains are incorporated (semi)coherently into the crystal lattice of the w-AlN columns with the epitaxial relation $\{111\}_{TiN}\langle 110\rangle_{TiN}//\{0001\}_{AlN}\langle 11\text{-}20\rangle_{AlN}$ developing the nanostructure shown in Figs. 4, 6 and 8. The co-existence of the parallel w-AlN⟨0001⟩ and c-TiN⟨111⟩ textures and the c-TiN⟨001⟩ texture in the first stage of film growth indicates that the crystals of these phases nucleated on the substrate and grew in strong competition controlled by their orientation dependent growth rates. This competition develops the textures in each phase, the ⟨001⟩ in the cubic and the ⟨0001⟩ in the wurtzite phase. This competition is followed by the competition of the ⟨001⟩ oriented c-TiN and ⟨0001⟩ oriented w-AlN crystals which is won by the ⟨0001⟩ oriented w-AlN phase. The structure developed by these processes is clearly present in sample ***B*** (Ti/Al-0.72, prepared by pulsed DC-MS) (Figs. 4, 5 and 6). Since the competition between the phases is controlled primarily by the relative number density of the

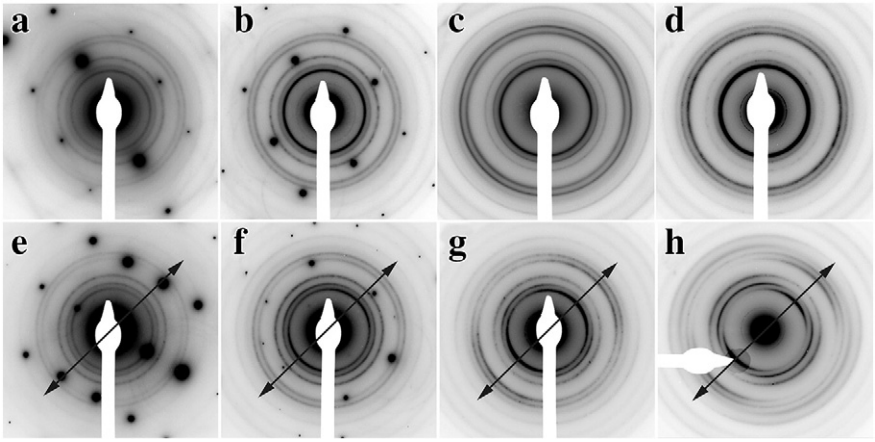

Fig. 15. Sample ***C***: SAED patterns taken on a plane-view specimen from areas located at successively increasing distances from the substrate: patterns (a)–(d) are taken at normal electron beam incidence, while (e)–(h) at tilted sample position (tilting angle ~20°). The axis of tilting is marked by arrows. (a) and (e) the very first thickness range near the Si substrate; (b) and (f) a thicker film on the substrate, (c) and (g) above the substrate, and (d) and (h) farther from the substrate.

nucleated crystals of cubic and wurtzite phases, the crossover thickness will decrease with increasing Al concentration as shown in Ref. [7].

However, results of samples ***B*** and ***C*** seem to be inconsistent with this conclusion. Namely they had the same Al content though the crossover thickness was much lower in sample ***C*** than in sample ***B***. This inconsistency can be dissolved by taking into account that the deposition parameters can sensitively affect the nucleation processes of the phases. The crossover thickness was about 0.6 μm in case of sample ***B***, deposited by asymmetric bipolar pulsed DC-MS, while it was only about 0.1 μm and not well pronounced in case of sample ***C***, prepared by DC-MS. Accordingly, the nucleation density of the c-TiAlN should be higher in sample ***B*** then it was in sample ***C*** at the same Al content. By this way one can suggest that the pulsed DC-MS promoted the formation of c-TiAlN nuclei.

Variation of the structure, first of all the decrease of the crossover thickness in the c-TiN phase, with increasing Al concentration in zone TW1 points to the possible existence of zone TW2, in which the texture crossover is completely missing and the c-TiN is present only with the <111> texture. That could be the situation when getting at the critical Al concentration at which only the supersaturated solid solution w-AlTiN phase nucleates on the substrate and the surface spinodal decomposition develops the Ti rich w-AlTiN and Al rich c-TiAlN nano-domains. The existence of TW2 had to be confirmed by dedicated experiments.

In the present experiments, applying oblique deposition, the single phase c-TiAlN films in zone S1 were grown with texture axis perpendicular to the substrate surface, while in case of w-AlTiN films in zone S2 the texture axis was tilted to the incidence angle of the vapour beam (not reported here). That is why in zone TW1 the axis of columns and the dominating c-TiN⟨001⟩ texture point to the substrate surface normal in the lower thickness range of the films, while the axis of columns and w-AlN⟨0001⟩//c-TiN⟨111⟩ textures are tilted to the vapour beam in the upper thickness range. The tilting of the column and texture axes of the w-AlN crystals to the direction of the vapour beam could be related to reduced surface adatom mobility.

5. Conclusions

For conclusion the following pathway of structure evolution can be proposed for $(Ti_{1-x}Al_X)_{1-y}Y_yN$ alloy films in the composition range of $0.72 < Ti/Al < 0.88$ with coexisting c-TiN⟨001⟩, w-AlN⟨0001⟩ and c-TiN ⟨111⟩ textures deposited in the temperature range corresponding to zone T of the temperature structure zone models.

- Randomly oriented crystals of the c-TiAlN and w-AlTiN type solid solution phases nucleate on the substrate. The chemical composition of these crystals could be near to the composition of the condensing vapour beam.
- c-TiAlN crystals grow as solid solution, while the w-AlTiN crystals partly decompose developing a c-TiN/w-AlN epitaxial nano-composite with (semi)coherent interfaces where $\{111\}_{TiN}\langle 110\rangle_{TiN}//\{0001\}_{AlN}\langle 11\text{-}20\rangle_{AlN}$.
- The incomplete coalescence of c-TiAlN and w-AlTiN crystals results in a continuous film constituted of randomly oriented crystals.
- The thickness growth of the continuous films proceeds by the competitive growth of randomly oriented crystals developing at first V-shaped columnar morphology in each phase and correspondingly the c-TiN⟨001⟩ and the coupled w-AlN⟨0001⟩//c-TiN⟨111⟩ textures.
- Following that, competition starts between the c-TiN⟨001⟩ crystals and the c-TiN/w-AlN epitaxial nano-composite crystals of w-AlN ⟨0001⟩ and c-TiN⟨111⟩ parallel orientations. This competition is won by the c-TiN/w-AlN epitaxial nano-composite crystals developing the single w-AlN⟨0001⟩//c-TiN⟨111⟩ texture fading out the c-TiN ⟨001⟩ crystals, appearing as an orientation crossover in the c-TiN phase.
- The film growth proceeds in the oriented growth regime of parallel sided columns of the c-TiN/w-AlN epitaxial nano-composite structure.

Acknowledgements

The authors acknowledge the financial support of the Hungarian Academy of Sciences under the grant number of OTKA-K81808. F. Misják also acknowledges the support by the János Bolyai Research Scholarship of the Hungarian Academy of Sciences.

References

[1] J. Pelleg, L.Z. Zevin, S. Lungo, N. Croitoru, Thin Solid Films 197 (1991) 117–128.
[2] U.C. Oh, J.H. Je, J.Y. Lee, J. Mater. Res. 10 (1995) 634.
[3] S. Mahieu, D. Depla, R. De Gryse, J. Phys. Conf. Ser. 100 (2008) 082003.
[4] M. Beckers, N. Schell, R.M.S. Martins, A. Mücklich, W. Möller, J. Vac. Sci. Technol. A23 (2005) 1384.
[5] A.R. Shetty, A. Karimi, Appl. Surf. Sci. 258 (2011) 1630.
[6] M. Moser, P.H. Mayrhofer, Scr. Mater. 57 (2007) 357.
[7] M. Moser, P.H. Mayrhofer, L. Székely, P.B. Barna, Surf. Coat. Technol. 203 (2008) 148–155.
[8] U. Wahlström, L. Hultman, J.E. Sundgreen, F. Abidi, I. Petrov, J.E. Greene, Thin Solid Films 235 (1993) 62.
[9] F. Abidi, I. Petrov, L. Hultman, U. Wahlström, T. Simizu, D. McItyre, J.E. Greene, J.E. Sundgreen, J. Appl. Phys. 69 (1991) 6437.
[10] D. Rafaja, Ch. Wüstefeld, D. Hegger, M. Šima, M. Jilek, Proc. 18th Plansee Seminar, Plansee Reutte HM, 49, 2013, pp. 1404–1413.
[11] G. Greczynski, J. Lu, J. Jensen, I. Petrov, J.E. Greene, S. Bolz, W. Kölker, Ch. Schiffers, O. Lemmer, L. Hultman, Thin Solid Films 556 (2014) 87–98. http://dx.doi.org/10.1016/j.tsf.2014.01.017.
[12] D. Rafaja, M. Šima, V. Klemm, G. Schreiber, D. Heger, L. Havela, R. Kužel, J. Alloys Compd. 378 (2004) 107–111.
[13] N. Schalk, C. Mitterer, J. Keckes, M. Penoy, C. Michotte, Surf. Coat. Technol. 209 (2012) 190.
[14] P.B. Barna, M. Adamik, Thin Solid Films 27–33 (1998) 317.
[15] I. Petrov, P.B. Barna, L. Hultman, J.E. Greene, J. Vac. Sci. Technol. A21 (2003) S117.
[16] P.B. Barna, G. Radnóczi, in: Katayun Barmak, Kevin Coffey (Eds.), Metallic films for electronic, optical and magnetic applications, Structure, processing and properties, Woodhead Publishing Series in Electronic and Optical Materials: Nr 40, 2014, pp. 67–120. http://dx.doi.org/10.1533/9780857096296.1.67.
[17] J.M. Nieuwenhuizen, H.B. Haanstra, Philips Tech. Rev. 27 (1966) 87.
[18] H. van Kranenburg, C. Lodder, Mater. Sci. Eng. R11 (1994) 295–354.
[19] S. Mahieu, P. Ghekiere, G. De Winter, R. De Gryse, D. Depla, G. Van Tendelo, O.I. Lebedev, Surf. Coat. Technol. 200 (2006) 2764–2768.
[20] R.G. Tissot, Powder Diffract. 18 (2003) 86–90.
[21] Hans J. Bunge, Helmut Klein, Z. Metallkd. 87 (6) (1996) 465–475.
[22] G.Z. Radnóczi, B. Pécz, J. Microsc. 224 (2006) 328–331.
[23] R. Manaila, A. Dévényi, D. Biro, L. David, P.B. Barna, A. Kovács, Surf. Coat. Technol. 151–152 (2002) 21.
[24] Ch. Wüstefeld, D. Rafaja, V. Klemm, C. Michotte, M. Kathrein, Surf. Coat. Technol. 205 (2010) 1345–1349.
[25] R. Cremer, M. Witthaut, A. von Richthofen, D. Neuschütz, Fresenius J. Anal. Chem. 361 (1998) 642–645.
[26] P. Patsalas, G. Abadias, G.M. Matenoglou, L.E. Koutsokeras, Ch.E. Lekka, Surf. Coat. Technol. 205 (2010) 1324–1330.
[27] P.J. Stadelman, Ultramicroscopy 21 (1987) 131.
[28] P.H. Mayrhofer, D. Music, J.M. Schneider, J. Appl. Phys. 100 (2006) 094906.
[29] R.F. Zhang, S. Veprek, Mater. Sci. Eng. A 448 (2007) 111.
[30] P.B. Hirsch, A. Howie, R.B. Nicholson, D.W. Pashley, M.J. Whelan, Electron Microscopy of Thin Crystals, Butterworth, London, 1965. 116–118.